Chinese Physics Letters

REVIEW

Novel Electronic Orders on the Kagome Lattice Near Van Hove Singularities

Cite as: Da Wang *et al*. 2026 *Chin. Phys. Lett.* **43** 060708

Special Topic: Kagome Materials

DOI CSTR

Recommended Articles

Three-Dimensional van Hove Singularities and Charge Density Wave Evolution in Kagome Lattice KV_3Sb_5
Yu Huang *et al*.
Chin. Phys. Lett. **42**, 120704 (2025)

Coexistence of near-E_F Van Hove Singularity and in-Gap Topological Dirac Surface States in Superconducting Electrides
Yin Yang *et al*.
Chin. Phys. Lett. **43**, 010708 (2026)

Electronic Instability of Kagome Metal CsV_3Sb_5 in the 2 × 2 × 2 Charge Density Wave State
Hongen Zhu *et al*.
Chin. Phys. Lett. **40**, (2023)

Flat Band and $_2$ Topology of Kagome Metal $CsTi_3Bi_5$
Yuan Wang *et al*.
Chin. Phys. Lett. **40**, (2023)

Discovery of Two Families of VSb-Based Compounds with V-Kagome Lattice
Yuxin Yang *et al*.
Chin. Phys. Lett. **38**, 127102 (2021)

Loop-Current Fluctuations Mediated Chiral *d*-Wave Pairing in Kagome Lattice
Qi-Fang Li, Gaopei Pan, Xu Zhang, Satoru Nakatsuji, Weilun Jiang, Xiao Yan Xu, and Xianxin Wu
Chin. Phys. Lett. **42**, 057302 (2025)

A series journal of Chinese Physical Society distributed by IOP Publishing

Chinese Physics Letters

Chin. Phys. Lett. **43** 060708 (2026)

REVIEW

DOI: 10.1088/0256-307X/43/6/060708
CSTR: 32039.14.0256-307X.43.6.060708

Novel Electronic Orders on the Kagome Lattice Near Van Hove Singularities

Da Wang(王达)[1,2], Wan-Sheng Wang(王万胜)[3], Meng Yao(姚猛)[1], Yi-Qun Liu(刘轶群)[1], Jia-Xin Yin(殷嘉鑫)[4], and Qiang-Hua Wang(王强华)[1,2,*]

[1]National Laboratory of Solid State Microstructures & School of Physics, Nanjing University, Nanjing 210093, China
[2]Collaborative Innovation Center of Advanced Microstructures, Nanjing University, Nanjing 210093, China
[3]Department of Physics, Ningbo University, Ningbo 315211, China
[4]Department of Physics, Southern University of Science and Technology, Shenzhen 518005, China

[*]Corresponding author. Email: qhwang@nju.edu.cn

The kagome lattice is unique in that Dirac bands, van Hove singularities, and flat band are all present in the band structure. In particular, the Bloch states near the upper van Hove points are sublattice polarized, while they are pair-wise mixed in sublattice contents near the lower van Hove points. These features, combined with correlation effects, may lead to novel electronic orders. We briefly review our theoretical investigations on the kagome lattice near the van Hove fillings by the singular-mode functional renormalization group, quantum Monte Carlo, and effective mean field theory. We establish rich phases of the model under extended Hubbard interactions or Su-Schrieffer-Heeger-like electron–phonon coupling. Among these phases, three types of 2 × 2 orders are of particular interest. Near the upper van Hove filling, we predicted the 2 × 2 charge bond order in 2013, which is highly relevant in AV_3Sb_5 (A = K, Rb, Cs) kagome materials. In the superconducting channel, we constructed a self-consistent theory for the 2 × 2 pair density wave, which is made possible by the sublattice polarization and attractive pairing interaction on the nearest neighbor bonds, predicting anisotropic energy gap in momentum space and quantized thermal Hall conductance in the chiral case of the pair density wave, which are consistent with recent photoemission and transport experiments. Near the lower van Hove filling, we further predicted a topological 2 × 2 non-collinear antiferromagnetic state with spins on neighboring sites orthogonal as Cartesian axes in three dimensions, which is a Chern insulator supporting quantized thermal Hall conductance.

Introduction

The kagome lattice is formed by vertex-shared triangles, with three sites per unit cell. The unique structure offers a platform for rich quantum states of matter. In the Mott insulating limit, the physics is described by the Heisenberg model, and the geometric frustration in the spin exchange may drive the system into quantum spin liquid states [1,2]. Away from the Mott limit, both in electron filling and electronic correlation, the model is also extensively discussed and a rich variety of electronic orders are proposed [3−8].

The free band structure contains Dirac points, van Hove singularities (vHS), and a flat band. When the Fermi level is at the vHS, the Fermi surface is perfectly nested and touches the van Hove points on the zone boundary. As usual, the logarithmic divergence in the density of states and the perfect nesting make the system extremely susceptible to electronic instabilities under electronic correlation. In comparison to the tight-binding model on a square lattice, where one may also meet the van Hove singularity and perfect nesting, the kagome lattice model is more intriguing because of the three sublattice degrees of freedom. The sublattice content of the Bloch states varies rapidly along the Fermi surface. If the Fermi level is on the upper vHS (closer to the flat band), the Bloch state is even polarized to one sublattice that rotates from one to the other van Hove points on the zone boundary. Such a vHS is defined as being p-type. On the other hand, if the Fermi level is at the lower vHS (on the far side of the flat band), the Bloch state on the van Hove point is pair-wise mixed in sublattice. Such a vHS is defined as being m-type. The two types of vHS are situated in energy symmetrically with respect to the Dirac point in the band structure, but the entire band is not particle-hoe symmetric because of the flat band. The sublattice polarization adds complexity into the competition between the possible electronic orders that would arise under correlation effect, and one may expect striking differences in the electron orders for the two types of vHS. Indeed, when the Fermi level is at the lower van Hove point, theory predicts a 2 × 2 non-collinear antiferromagnetic (AFM) state, which is also a Chern insulator [9]. At the upper van Hove level, theory predicts, apart from the more conventional charge/spin density waves, the 2 × 2 valence bond solid, or charge bond order (CBO) [10,11]. When this order is leading, it is found that the second-leading ordering tendency is the 2 × 2 pair density wave (PDW) state (rather than the more conventional zero-momentum pairing), thanks to the sublattice polarization [12]. Recently, the interest in the kagome model near the vHS is greatly enhanced by the experiments in the AV_3Sb_5 (A = K, Rb, Cs) kagome materials [3–8,13−16], where a 2 × 2 charge order is indeed observed, although there are still debates on whether it is a loop current order (an imaginary version of the CBO) [17−23]. Moreover, the 2 × 2 PDW state is also reported and discussed [24,25]. These experimental progresses call for a better and more comprehensive understanding of the single-orbital kagome model as a minimal model for the AV_3Sb_5 and other kagome materials.

Here we review our studies on the kagome lattice near the van Hove levels [9,10,12,26]. Some parallel results in the literature are also discussed. In the remaining part of the paper: (i) We introduce the model; (ii) We review the results of the extended Hubbard model in the case of p-type vHS; (iii) We review our results for the kagome model subject to electron–phonon coupling, where the phonon mode modulates the electron hopping on nearest-neighbor bonds; (iv) We review the results for the m-type vHS with local Hubbard interaction; (v) We review the self-consistent mean field theory for possible electronic orders and properties that might be relevant in the AV_3Sb_5 kagome materials; (vi) Finally, we provide a summary of the results, and some perspectives on theoretical as well as experimental aspects.

Received 11 March 2026; accepted 24 April 2026; published 1 July 2026
© 2026 Chinese Physical Society and IOP Publishing Ltd. All rights, including for text and data mining, AI training, and similar technologies, are reserved.

Check for updates

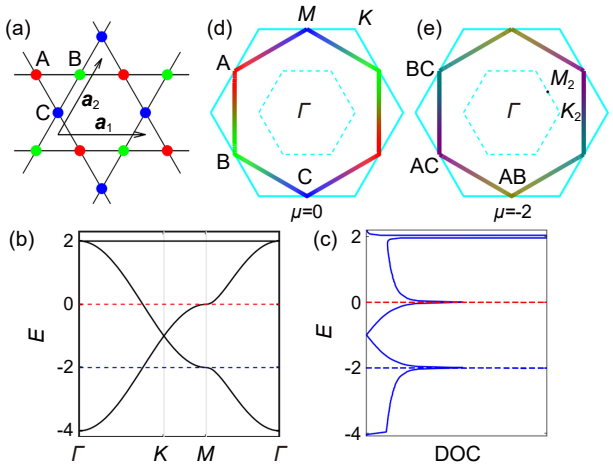

Fig. 1. (a) Plots the kagome lattice with A/B/C indicating three sublattices. $\boldsymbol{a}_1$ and $\boldsymbol{a}_2$ are two primitive translation vectors. (b) Plots the band dispersion along the high symmetry path $\Gamma-K-M-\Gamma$. (c) Plots the density of states (DOS). The dashed lines in (b) and (c) indicate two van Hove fillings. As shown in (b) and (c), t is taken as the energy unit. The Fermi surfaces at the upper (p-type) and lower (m-type) van Hove fillings are shown in (d) and (e), respectively, for which the colors encode the sublattice contents. The small hexagons are reduced Brillouin zones in the case of enlarged 2 × 2 super unit cell. Adapted from Ref. [12].

Model

The kagome lattice is shown in Fig. 1(a), containing three sublattices (denoted by A, B, and C, respectively) in each unit cell. Its electronic structure contains some fascinating properties even for the simplest case, i.e., single orbital tight-binding model described by the free Hamiltonian

$$H_0 = -t\sum_{\langle ij\rangle\sigma}\left(c^\dagger_{i\sigma}c_{j\sigma}+\text{h.c.}\right)-\mu\sum_i n_i, \tag{1}$$

where t is the hopping integral on nearest-neighbor bonds, $c^\dagger_{i\sigma}$ creates an electron at site-i with spin σ, $\langle ij\rangle$ denotes the nearest neighboring bonds, μ is the chemical potential, and $n_i=\sum_\sigma c^\dagger_{i\sigma}c_{i\sigma}$. The band dispersion and density of states are shown in Figs. 1(b) and 1(c), respectively. The band structure exhibits a flat band at $E=2t$, two Dirac points at $E=-t$ and two van Hove fillings at $E=0$ and $-2t$. As usual, the logarithmic divergence in the density of states at the van Hove fillings indicates the system is highly susceptible to electronic instabilities under correlation effect. Here, more complexities come from the nested Fermi surfaces with distinct sublattice polarizations for these two van Hove fillings, as shown in Figs. 1(d) and 1(e), respectively. The sublattice contents on the Fermi surfaces are encoded by the colors corresponding to the three sublattices as shown in Fig. 1(a). At the upper van Hove filling, the Bloch wave function at each van Hove point M_i is contributed by only one sublattice, hence, called p-type. On the other hand, at the lower van Hove filling, the Bloch wave function at each M_i is pair-wise mixed in sublattice, hence, called m-type. Such distinct sublattice polarizations lead to quite different electronic instabilities under correlation effect near these two van Hove fillings as shown below.

Electronic Orders at the P-Type vHS

At the upper p-type van Hove filling, we investigated the extended Hubbard model

$$H_H = H_0 + U\sum_i n_{i\uparrow}n_{i\downarrow}+V\sum_{\langle ij\rangle}n_in_j, \tag{2}$$

where U is the onsite Hubbard repulsion and V is the Coulomb interaction between the nearest neighboring bonds. Employing singular mode functional renormalization group (SM-FRG) method [27,28], we established the first complete phase diagram of the extended Hubbard model versus U and V at the upper van Hove filling [10], as shown in Fig. 2(a). Concurrently, other groups investigated the same model from different approaches, with some difference in the conclusions [11,29] indicating the subtlety of this problem. Very recently, however, the same European group revisited this problem with improved calculations and confirmed our original findings [30].

In the weak interaction limit, the electronic instability can be understood by the Stoner criterion. Since the DOS is divergent at the van Hove filling, any finite attractive interaction tends to induce instability at zero momentum. The Hubbard U is attractive in spin channel, and thus favors ferromagnetism (FM) as usual. While the nearest neighbor Coulomb interaction V is attractive in the density channel and thus favors site-centered charge density wave (CDW). Note that this CDW has zero momentum and is invariant across unit cells. Moreover, it contains two degenerate modes forming a two-dimensional representation, as depicted in Figs. 2(b) and 2(c), with up/down arrows representing the positive/negative charge deviation, respectively.

With increasing U up to an intermediate range for small V, the instability still occurs in the spin density wave (SDW) channel at zero momentum but the leading FM mode changes to a two-dimensional representation with two degenerate modes, still depicted in Figs. 2(b) and 2(c) but with arrows representing spin density now. In this regime, mean field calculation helps us to pin down the ground state as a planar 120°-AFM order as shown in Fig. 2(d). By further increasing U, we enter a CBO phase, where the hopping integral is modulated, with three degenerate modes corresponding to the three van Hove points M_i, respectively. In the ordered state, the three modes further combine together to form the star-of-David pattern as shown in Fig. 2(e), with thick/thin bonds representing the stronger/weaker hopping. The predicted 2 × 2 structure of the charge order is seen in the AV_3Sb_5 kagome materials, although it is speculated that the time-reversal symmetry is further broken [17–23]. The latter can be viewed as the imaginary counterpart of the CBO. Early theoretical proposals based on vHS analysis and phenomenological Landau theory have suggested the possibility of such a loop current order [31–34]. Recently, it has been argued that longer-ranged Coulomb interactions may stabilize this order [35], since the susceptibility involving only next-nearest-neighbor fermion bilinears is found to favor the loop current order [36], as supported by a recent FRG study on a spinless model with large next-nearest-neighbor Coulomb repulsion [37]. However, in our simulations based on a spinful model, we do not observe the loop current order in physically realistic parameter regimes. Thus, there remains no consensus on this issue, and further studies are needed to resolve the conditions under which this exotic order may emerge for a spinful model. Besides the above charge and spin orders, s-wave and d-wave superconductivity orders are also stabilized with increasing V before the site-centered CDW phase enters eventually.

Effect of Electron–Phonon Coupling

We further investigated the effect of bond phonon coupling to electron hopping, called Su-Schrieffer-Heeger (SSH) electron–phonon interaction defined as

$$H_{\text{SSH}} = H_0+\sum_{\langle ij\rangle}gx_{\langle ij\rangle}(c^\dagger_{i\sigma}c_{j\sigma}+\text{h.c.})+\omega a^\dagger_{\langle ij\rangle}a_{\langle ij\rangle}, \tag{3}$$

where $x_{\langle ij\rangle}=(a_{\langle ij\rangle}+a^\dagger_{\langle ij\rangle})/\sqrt{2M\omega}$ represents the displacement of the phonon mode on bond $\langle ij\rangle$ and $a_{\langle ij\rangle}$ is the standard phonon annihilation operator. The SSH electron–phonon interaction has become a research interest in recent years since it favors several types of electronic orders other than only the usual superconductivity [38–40]. On the kagome lattice, we combined SM-FRG to treat the phonon induced retarded interaction [41] and determinant quantum Monte Carlo (DQMC) [42] to study the SSH model on the kagome lattice [26]. The results are summarized in the phase diagram versus the phonon frequency ω and dimensionless electron–phonon interaction constant

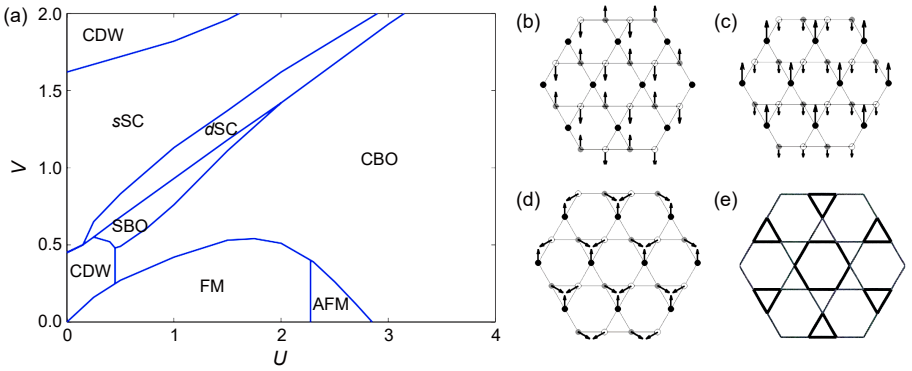

Fig. 2. (a) Phase diagram of the extended Hubbard model at the upper (p-type) van Hove filling. (b) and (c) Present two degenerate CDW or SDW modes (uniform across unit cells), with the arrows indicating net charge or spin densities, respectively. (d) Shows the particular planar 120°-AFM obtained by mean field calculation by linearly combining the two degenerate modes in (b) and (c). (e) Presents the 2 × 2 star-of-David CBO with thick/thin lines denoting strong/weak charge bonds. Adapted from Ref. [10].

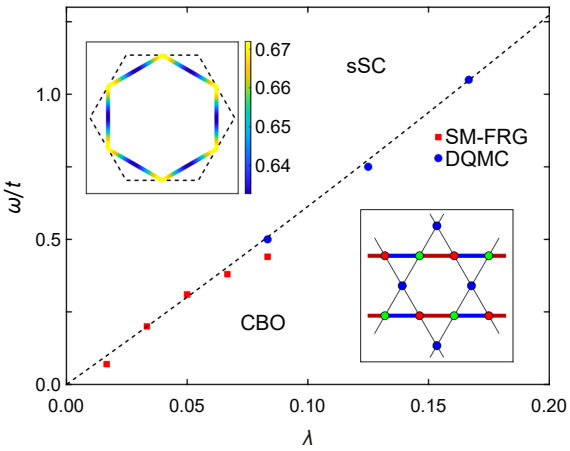

Fig. 3. Phase diagram of the SSH electron phonon coupling model at the upper (p-type) van Hove filling, with ω the phonon frequency and λ the dimensionless electron–phonon coupling constant, see main text for definition. The top left inset shows the gap function on the Fermi surface, and the bottom right inset shows one eigen mode of the CBO order with red/blue lines indicating strong/weak charge bonds. Adapted from Ref. [26].

$\lambda = g^2/6tM\omega^2$, as shown in Fig. 3. For high frequency phonon with weak λ, the SSH phonon is found to mediate the usual s-wave superconductivity (sSC). This is because the phonon mediates attractive pair hopping from one site to the other on the bond, leading to onsite pairing. But for low-frequency phonon with strong λ, the system enters the 2 × 2 CBO phase, which is an analogue of the Peierls instability. Therefore, the experimentally observed charge order may also originate from the electron–phonon coupling, serving as an alternative mechanism other than pure electronic correlation for the charge order in kagome materials. Note that although the phonon modes on the kagome lattice has been extensively studied [43], their effect on the electronic orders has been rarely studied [44,45] and calls for further exploration.

Electronic Orders at the M-Type vHS

At the lower van Hove filling, we combined SM-FRG and variational Monte Carlo (VMC) [46] to obtain the phase diagram of the pure Hubbard model with $V = 0$ [9], as shown in Fig. 4(a). Similar to the upper van Hove filling, small U induces the usual FM order following the Stoner criterion. As U increases, the system is found to enter a 2 × 2 SDW order with three degenerate modes at three M_i. By FRG-derived mean field calculations, the ground state is identified as an antiferromagnetism with three neighboring spins all orthogonal to each other as the Cartesian axes in three dimensions, hence, called 90°-AFM state. Interestingly, such a non-collinear magnetic order is topologically nontrivial, exhibiting nonzero Chern number as shown in the cylindrical band structure in Fig. 4(b). As a result, it is in fact a Chern insulator supporting quantized thermal Hall conductance. By further increasing U, the system finally gets back to the FM state, which is different from the 2 × 2 CBO obtained at the upper van Hove filling. The FM state in the large U limit arises from the spin-polarization induced kinetic energy gain [47] for the pair-wise sublattice polarization. For comparison, the pure sublattice polarization at the upper p-type vHS forbids such a mechanism for FM re-entrance.

PDW Near the P-Type vHS

Finally, let us focus on superconductivity without restricting to the above particular microscopic correlation models. At the van Hove fillings, the divergent DOS comes from the van Hove points. Hence, the low energy physics can be effectively captured by considering the three vHS points M_i. At the upper p-type van Hove filling, as shown in Fig. 1(d), the Bloch wave function at M_i is extremely sublattice polarized. This dictates that the usual zero-momentum Cooper pairing can only come from the same sublattice. Under this restriction, if the onsite pairing is suppressed by e.g. Hubbard U, the on-bond (nearest or next-nearest neighbor) pairings from different sublattices have to connect different vHS points, leading to nonzero total pairing momentum M_i, since addition of any two inequivalent vHS momenta equals the third one up to a reciprocal vector. This inspires us to construct 2 × 2 PDW orders [12], as a natural realization of the Fulde–Ferrell–Larkin–Ovchinnikov (FFLO) state but without resorting to applying magnetic field [48]. As a comparison, at the lower van Hove filling, there is no such a particular sublattice selection rule to forbid the usual zero-momentum Cooper pairing. The above physical analysis can be quantitatively visualized in the pair-pair susceptibility $\chi(\boldsymbol{q})$ with the matrix element $\chi_{IJ}(\boldsymbol{q}) = (1/L^4)\sum_{ij}\int_0^\beta d\tau\langle b_{iI}(\tau)b^\dagger_{jJ}(0)\rangle \exp(i\boldsymbol{q}\cdot(\boldsymbol{r}_j - \boldsymbol{r}_i))$ where $b_{iI} = c_{i+\delta_I\downarrow}c_{i+\delta'_I\uparrow}$ denotes the I-th bond pairing operator. The leading eigenvalue of $\chi(\boldsymbol{q})$ is plotted in Fig. 5(a) for both van Hove fillings. At the upper p-type vHS, the largest eigenvalue appears at $\boldsymbol{q} = M$, indicating the PDW instability is indeed mostly favorable, winning over the usual Cooper pairing. In the right inset, the temperature dependence of the leading eigenvalue at M is plotted, exhibiting the logarithmic divergence arising from the divergent DOS. Instead, as a comparison, it can be seen that near the lower m-type van Hove filling, the leading eigenvalue appears at $\boldsymbol{q} = 0$, favoring the usual Cooper paring.

For the 2 × 2 PDW instability at p-type vHS, there are three degenerate PDW modes ψ_i corresponding to three M_i points, with one mode shown in the left inset in Fig. 5(a). At the phenomenological level, we construct a three-component Ginzburg-Landau (GL) free energy.

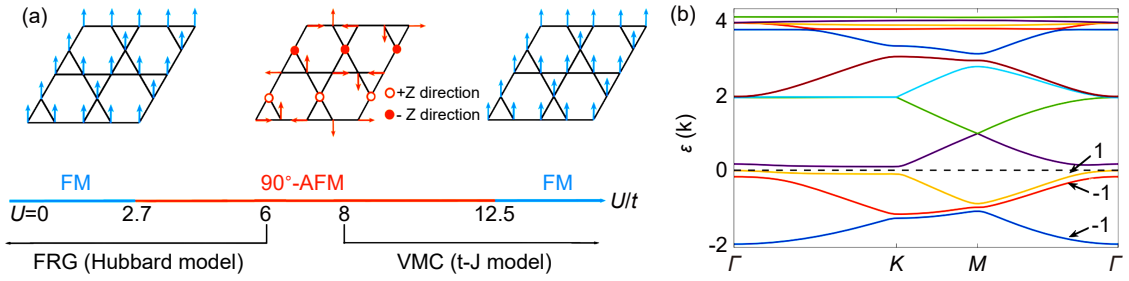

Fig. 4. (a) Phase diagram of the Hubbard model at the lower (m-type) van Hove filling. The spin configurations of the two phases are sketched in the above correspondingly. (b) For the intermediate 90°-AFM state, the ground state is an anomalous Chern insulator with the Chern number explicitly shown for each filled bands. Adapted from Ref. [9].

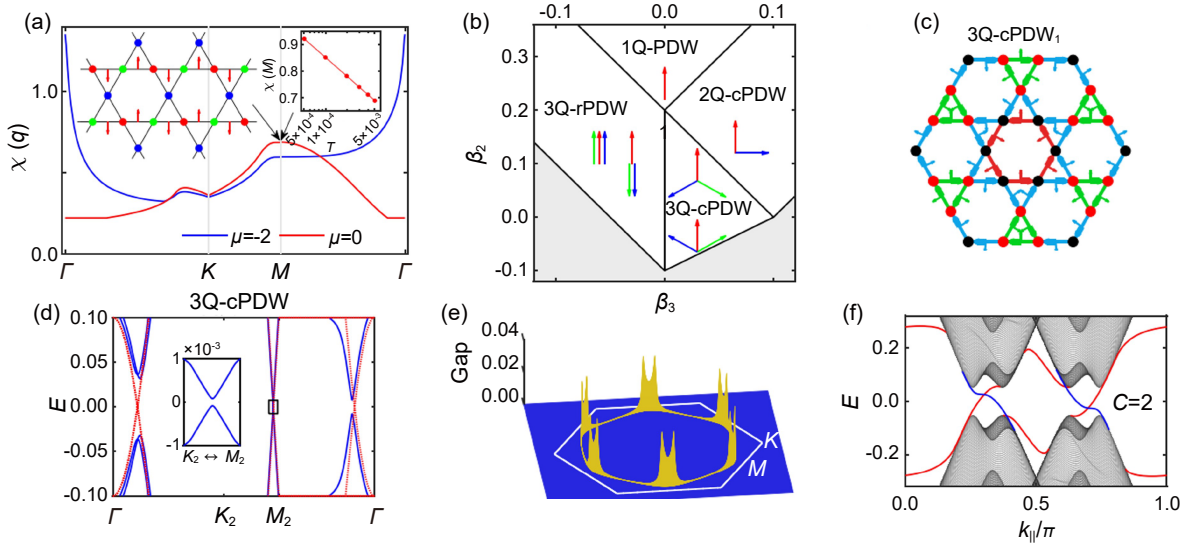

Fig. 5. (a) Leading pair susceptibility with only on-bond pairings at the upper ($\mu = 0$) and lower ($\mu = -2$) van Hove fillings. The left inset gives the eigen mode at one vHS point M for the upper van Hove filling. The right inset plots the leading eigen value of $\chi(M)$ versus temperature, exhibiting a logarithmic divergence. (b) GL phase diagram of the 2×2 PDW state versus GL parameters β_2 and β_3 by fixing $\beta_1 = 0.1$. The amplitudes and phases of different order parameter components are indicated by the lengths and directions of the arrows. (c) A typical example of the 3Q-cPDW pattern with arrows along each bond representing the emerged loop current and the other arrows indicating the pairing phases. For this specific chiral 3Q-cPDW order, the Bogoliubov-de Gennes (BdG) energy spectrum and quasiparticle gap slightly doping away from the van Hove filling are given in (d) and (e), respectively. (f) We plot the energy spectrum with an artificially large gap value on a cylinder with open boundaries along the $\boldsymbol{a}_1$ direction, exhibiting two gapless edge states on each boundary (red or blue), consistent with the total Chern number $C = 2$. Adapted from Ref. [12].

$$F_{\mathrm{PDW}} = -\alpha \sum_{i=1}^{3} |\psi_i|^2 + \beta_1 \sum_{i=1}^{3} |\psi_i|^4 + \beta_2 \sum_{i<j} |\psi_i|^2 |\psi_j|^2 + \beta_3 \sum_{i<j} (\psi_i^{*2} \psi_j^2 + \mathrm{h.c.}) + \cdots , \tag{4}$$

where we omit all higher order and gradient terms. By varying β_2 and β_3, we can obtain 1Q, 2Q, and 3Q PDW states given by the number of nonzero components ψ_i, see Fig. 5(b). For the 3Q PDW states, the three components may have the same phase, called 3Q-rPDW, or have relative phase differences ($\pi/6$ or $\pi/3$), called 3Q-cPDW. By mean field calculations, we can indeed obtain different types of PDW states. One example of 3Q-cPDW is shown in Fig. 5(c) with arrows (orthogonal to bonds) indicating the phases of on-bond pairings. Interestingly, it is found that the 3Q-cPDW phase exhibits both 2×2 real and imaginary CBO automatically, suggesting these two types of orders are strongly intertwined together.

We next focus on the properties of the novel chiral 3Q-cPDW order. The low energy BdG quasiparticle band is plotted in the reduced Brillouin zone in Fig. 5(d). The energy spectrum is fully gapped but the gap minimum is quite small, which can be understood by high-order degenerate perturbation theory, i.e. any $\boldsymbol{k}$ on the Fermi surface can be scattered subsequently by three M_i-pairings to $M_3 - [M_2 - (M_1 - \boldsymbol{k})] = -\boldsymbol{k}$ (since $\pm M_1 \pm M_2 \pm M_3 = 0$ up to reciprocal vectors) which is still on the Fermi surface. Such a scattering process can break the degeneracy and open a quasiparticle gap at the Fermi level. However, in real experiments, such a small gap is difficult to resolve and thus may lead to a "residual Fermi surface" as shown in Fig. 5(e), resembling the "Fermi arc" or "Bogoliubov Fermi surface". This property can be used to distinguish the chiral PDW from the usual superconductivity. As a result of the "residual Fermi surface", quasiparticle interference patterns [49] can be observed, as reported in a recent experiment [25]. Actually, the strong anisotropic gap has been directly observed by angle-resolved photoemission spectroscopy (ARPES) measurement [50]. On the other hand, since the 3Q-PDW state is fully gapped, its Chern number is theoretically well defined, which is found to be zero for the real PDW case and ±2 for the chiral PDW case. In Fig. 5(f), the energy spectrum on a cylinder is presented, exhibiting two gapless edge modes on each boundary. In principle, such chiral edge states are expected to yield quantized thermal Hall conductance, which may be consistent with a recent experiment [51].

Summary and Perspectives

In this paper, we briefly review our theoretical results on the kagome lattice based on correlated electronic model calculations. Near the van Hove fillings, rich phases are established, among which three types of 2×2 orders are particularly interesting. In the charge

channel, the 2 × 2 CBO near the upper p-type vHS [10] is believed to be relevant in AV_3Sb_5 kagome materials in an imaginary version, the loop current order [19]. In the spin channel, the non-collinear 2 × 2 SDW (90°-AFM) at the lower m-type vHS [9] is a Chern insulator supporting quantized thermal Hall conductance. In the superconducting channel, the 2 × 2 PDW near the upper p-type vHS is likely to win over the conventional uniform superconducting state thanks to the sublattice polarization and onsite repulsion [12]. This PDW yields highly anisotropic energy gap along the Fermi surface, and is a topological superconductor supporting quantized thermal Hall conductance. The high gap anisotropy and thermal Hall conductance are consistent with the recent experiments [25,50,51]. Of course, in realistic kagome materials, there are additional complexities arising from multi-orbitals crossing the Fermi level and the presence of more than one vHS within the low energy window [52−55]. These factors are needed in future studies for closer comparison to experiments.

Acknowledgments

This work was supported by the National Key R&D Program of China (Grant Nos. 2022YFA1403201 and 2024YFA1408104) and the National Natural Science Foundation of China (Grant Nos. 12374147, 12274205, and 92365203).

References

[1] Norman M R 2016 *Rev. Mod. Phys.* **88** 041002
[2] Zhou Y, Kanoda K, and Ng T K 2017 *Rev. Mod. Phys.* **89** 025003
[3] Yin J X, Lian B, and Hasan M Z 2022 *Nature* **612** 647
[4] Neupert T, Denner M M, Yin J X, Thomale R, and Hasan M Z 2022 *Nat. Phys.* **18** 137
[5] Jiang K, Wu T, Yin J X, Wang Z Y, Hasan M Z, Wilson S D, Chen X H, and Hu J P 2023 *Natl. Sci. Rev.* **10** nwac199
[6] Wang Y J, Wu H, McCandless G T, Chan J Y, and Ali M N 2023 *Nat. Rev. Phys.* **5** 635
[7] Wilson S D and Ortiz B R 2024 *Nat. Rev. Mater.* **9** 420
[8] Di Sante D, Neupert T, Sangiovanni G *et al*. 2026 *Rev. Mod. Phys.* **98** 015002
[9] Liu Y Q, Liu Y B, Wang W S, Wang D, and Wang Q H 2024 *Phys. Rev. B* **109** 075127
[10] Wang W S, Li Z Z, Xiang Y Y, and Wang Q H 2013 *Phys. Rev. B* **87** 115135
[11] Kiesel M L, Platt C, and Thomale R 2013 *Phys. Rev. Lett.* **110** 126405
[12] Yao M, Wang Y, Wang D, Yin J X, and Wang Q H 2025 *Phys. Rev. B* **111** 094505
[13] Ortiz B R, Gomes L C, Morey J R *et al*. 2009 *Phys. Rev. Mater.* **3** 094407
[14] Ortiz B R, Teicher S M L, Hu Y *et al*. 2020 *Phys. Rev. Lett.* **125** 247002
[15] Ortiz B R, Sarte P M, Kenney E M, Graf M J, Teicher S M L, Seshadri R, and Wilson S D 2021 *Phys. Rev. Mater.* **5** 034801
[16] Liu Y, Liu Z Y, Bao J K *et al*. 2024 *Nature* **632** 1032
[17] Li H X, Zhang T T, Yilmaz T *et al*. 2021 *Phys. Rev. X* **11** 031050
[18] Ortiz B R, Teicher S M L, Kautzsch L *et al*. 2021 *Phys. Rev. X* **11** 041030
[19] Jiang Y X, Yin J X, Denner M M *et al*. 2021 *Nat. Mater.* **20** 1353
[20] Liang Z W, Hou X Y, Zhang F *et al*. 2021 *Phys. Rev. X* **11** 031026
[21] Zhao H, Li H, Ortiz B R *et al*. 2021 *Nature* **599** 216
[22] Li H, Zhao H, Ortiz B R, Park T, Ye M X, Balents L, Wang Z Q, Wilson S D, and Zeljkovic I 2022 *Nat. Phys.* **18** 265
[23] Le T, Pan Z M, Xu Z K *et al*. 2024 *Nature* **630** 64
[24] Chen H, Yang H T, Hu B *et al*. 2021 *Nature* **599** 222
[25] Deng H B, Qin H L, Liu G W *et al*. 2024 *Nature* **632** 775
[26] Yang Q G, Yao M, Wang D, and Wang Q H 2024 *Phys. Rev. B* **109** 075130
[27] Metzner W, Salmhofer M, Honerkamp C, Meden V, and Schönhammer K 2012 *Rev. Mod. Phys.* **84** 299
[28] Wang W S, Xiang Y Y, Wang Q H, Wang F, Yang F, and Lee D H 2012 *Phys. Rev. B* **85** 035414
[29] Yu S L and Li J X 2012 *Phys. Rev. B* **85** 144402
[30] Profe J B, Klebl L, Grandi F *et al*. 2024 *Phys. Rev. Res.* **6** 043078
[31] Feng X, Jiang K, Wang Z, and Hu J P 2021 *Sci. Bull.* **66** 1384
[32] Denner M M, Thomale R, and Neupert T 2021 *Phys. Rev. Lett.* **127** 217601
[33] Lin Y P and Nandkishore R M 2021 *Phys. Rev. B* **104** 045122
[34] Park T, Ye M X, and Balents L 2021 *Phys. Rev. B* **104** 035142
[35] Dong J W, Wang Z Q, and Zhou S 2023 *Phys. Rev. B* **107** 045127
[36] Fu R Q, Zhan J, Dürrnagel M *et al*. 2025 *Natl. Sci. Rev.* **12** nwaf414
[37] Zhan J, Hohmann H, Dürrnagel M *et al*. 2026 *Phys. Rev. Lett.* **136** 126001
[38] Cai X, Li Z X, and Yao H 2021 *Phys. Rev. Lett.* **127** 247203
[39] Xing B, Chiu W T, Poletti D, Scalettar R T, and Batrouni G 2021 *Phys. Rev. Lett.* **126** 017601
[40] Yang Q G, Wang D, and Wang Q H 2022 *Phys. Rev. B* **106** 245136
[41] Wang D, Wang W S, and Wang Q H 2015 *Phys. Rev. B* **92** 195102
[42] Noack R M, Scalapino D J, and Scalettar R T 1991 *Phys. Rev. Lett.* **66** 778
[43] Chen H, Wu W K, Yang S Y A, Li X, and Zhang L F 2019 *Phys. Rev. B* **100** 094303
[44] You J Y, Hsu C E, Del Ben M, and Li Z L 2025 *Phys. Rev. Lett.* **134** 106401
[45] Liu L Y, Li Y D, Tan H X *et al*. 2026 *Natl. Sci. Rev.* **13** nwag044
[46] Becca F and Sorella S 2017 *Quantum Monte Carlo Approaches for Correlated Systems* (Cambridge University Press)
[47] Pollmann F, Fulde P, and Shtengel K 2008 *Phys. Rev. Lett.* **100** 136404
[48] Agterberg D F, Davis J C S, Edkins S D *et al*. 2020 *Annu. Rev. Condens. Matter Phys.* **11** 231
[49] Wang Q H and Lee D H 2003 *Phys. Rev. B* **67** 020511
[50] Mine A, Zhong Y G, Liu J J *et al*. 2025 *Commun. Mater.* **6** 276
[51] Yoshida H, Takeda H, Yan J *et al*. 2025 *Sci. Adv.* **11** eadu2973
[52] Cho S H, Ma H Y, Xia W *et al*. 2021 *Phys. Rev. Lett.* **127** 236401
[53] Hu Y, Wu X X, Ortiz B R *et al*. 2022 *Nat. Commun.* **13** 2220
[54] Kang M, Fang S, Kim J K *et al*. 2022 *Nat. Phys.* **18** 301
[55] Lan Y J, Lei Y H, Le C C *et al*. 2026 *Phys. Rev. Lett.* **136** 016401